Article

Photocatalytic Bactericidal Performance of LaFeO₃ under Solar Light: Kinetics, Spectroscopic and Mechanistic Evaluation

Nazmiye Cemre Birben [1], **Ezgi Lale** [1], **Renato Pelosato** [2], **Ceyda Senem Uyguner Demirel** [1], **Isabella Natali Sora** [2,*] **and Miray Bekbolet** [1]

1   Institute of Environmental Sciences, Bogazici Univresity, 34342 Istanbul, Turkey;
    cemre.birben@boun.edu.tr (N.C.B.); ezgilale91@gmail.com (E.L.); uygunerc@boun.edu.tr (C.S.U.D.);
    bekbolet@boun.edu.tr (M.B.)
2   INSTM and Department of Engineering and Applied Sciences, University of Bergamo, 24044 Dalmine, Italy;
    renato.pelosato@unibg.it
*   Correspondence: isabella.natali-sora@unibg.it

Abstract: Lanthanum orthoferrites are a versatile class of catalysts. Here, the photocatalytic bactericidal performance of LaFeO₃ (LF) to inactivate pathogenic microorganisms, i.e., *Escherichia coli* (*E. coli*), in water under simulated solar irradiation conditions was investigated. Various competing and contributing factors were covered to visualize the reaction medium consisting of *E. coli* K12 cells, organic sub-fractions formed by cell destruction, and LF surface. LF solar photocatalytic inactivation (SPCI) kinetics revealed the highest inactivation rate in ultrapure water as expected, followed by distilled water (DW), aqueous solution containing anions and cations (WM) and saline solution (SS). Characterization of the released organic matter was achieved by UV-vis and fluorescence spectroscopic techniques as well as organic carbon contents (DOC). Upon SPCI, significant amounts of K⁺ along with released protein contents were detected expressing cell wall destruction and lysis. Under the specified experimental conditions, in the presence of released intracellular organic and inorganic components via cell lysis, a significant count of *E. coli* was still present in SS, whereas almost all bacteria were removed in other matrices due to various challenging reasons. Based on the presented data, SPCI of *E. coli* using LF as a novel photocatalyst was successfully demonstrated as an alternative and promising method for disinfection purposes.

Keywords: *E. coli*; lanthanum orthoferrite; perovskite; photocatalytic inactivation

1. Introduction

Microbial contamination in drinking water is a serious concern in many low-income countries. Pathogenic microorganisms present in water mainly include viruses, bacteria, parasites, etc. Diseases related to contamination of drinking water constitute a major problem for human health. Therefore, it is necessary to develop processes of microbial disinfection of water that combine high efficiency with simplicity of management and cost-effectiveness. Generally, microbial disinfection of water is achieved through chlorination, ozonation, chloramination, the use of chlorine dioxide or UV radiation [1,2]. Among the disinfection processes that are used in smaller-scale systems, photocatalysis is widely studied. The most studied photocatalyst is titanium dioxide (TiO₂), which is proven to be particularly effective due to its good chemical and environmental stability and strong oxidizing power of the holes [3,4]. When TiO₂, suspended in water, is irradiated with UV light, hydroxyl radicals are generated. These promote the oxidation of the organic substances and/or the inactivation of pathogenic microorganisms, such as bacteria, viruses and parasites.

The catalysts alternative to TiO₂ display different crystalline structures such as perovskites (ABO₃), perovskite-related materials, ABO₄ compounds with scheelite structures (such as some tungstates, molybdates or vanadates) and iron spinels (AB₂O₄). Briefly,

perovskite structure with the general formula ABO_3, where A cation can be a lanthanide, alkaline, or alkaline-earth cation, while B cation is a metallic element from the *d*-block, are stable structures, which could form solid solutions with a range of metal ions. Perovskites could be good candidates for replacing TiO_2 by extending the light absorption range to the visible region, thereby maintaining successful utilization of solar light [5]. Rojas-Cervantes and Castillejas published a review paper covering literature findings on the use of perovskites as catalysts in advanced oxidation processes (AOP) for wastewater treatment [6].

Although a significant number of studies are available on the preparation and use of perovskites as efficient photocatalysts for the removal of pollutants, a literature survey shows few papers reporting on antimicrobial activity rather than photocatalytic activity [7,8]. Among the environmentally sound water remediation technologies, Ag-$La_{0.8}Ca_{0.2}Fe_{0.94}O_{3-\delta}$ perovskite activated via catalytic peroxymonosulfate was described [9]. Antimicrobial activities were assessed for synthesized photocatalysts such as $Bi_{1-x}Al_xFeO_3$ ($0.0 \leq x \leq 0.15$), $CoFeO_4$, Er-LiNiferrite, $LaCo_{1-x}Fe_xO_3$, $ZnLaFe_2O_4/NiTiO_3$ and $SrTi_{1-x}Fe_xO_{3-\sigma}$ [10–15]. Mostly, bacteria were used as examples of G(−) bacteria: *E. coli*, *Campylobacter jejuni*, *Klebsiella phemoniae*, *Pseudomonas aeruginosa* and *Vibrio cholerae*, and of G(+) bacteria: *Staphlococcus aureus*, *Listeria monocytogenes* and *Bacillus subtilis*. *Candida albicans* was also used as an example of yeast [16,17].

The peroxidation of the polyunsaturated phospholipid component of lipid membrane in the cells is the main mechanism of bacteria inactivation, since vital activities that depend on intact cell membrane, such as respiratory activity, are lost. Zhang and co-workers synthesized a novel $SrTi_{1-x}Fe_xO_{3-\sigma}$ photocatalyst [15]. In their paper, the mechanistic explanation was based on metal oxide–bacteria interaction; moreover, various operational parameters like pH effect and particle size, as well as the role of released compounds, were also discussed. Photocatalytic treatment using fluorescent light with yellow filters was found to be very efficient as 5 log *E. coli* inactivation was achieved in 15 min of the irradiation period. Moreover, similar performance was also noticed under dark conditions that was attributed to mechanical action, thereby excluding the photocatalytic removal mechanism.

Among the perovskite oxides, $LaFeO_3$ (LF) has gained considerable interest due to its easy synthesis combined with large chemical stability, low-cost and non-toxicity. Several applications like gas sensors [18,19], catalyst [20,21] and pollution remediation [8,22] have been explored for LF. Furthermore, LF is a p-type semiconductor which possesses a relatively narrow band-gap energy around 2.5 eV [23]. It is proposed as visible-light and UV photocatalyst for aqueous reactions [8,24–27], often combined with a Fenton-like reaction [28,29]. As many perovskite-type oxides, LF shows a high recombination rate of photogenerated electron–hole (e_{CB}^- and h_{VB}^+) pairs [30]. Several strategies are developed to reduce the unfavorable electron–hole recombination process, such as doping with transition metal elements [22,31], fabrication of heterojunction-composite [32,33] and decoration with Ag [34]. However, these solutions of the problem show inherent drawbacks, such as lower chemical stability with respect to the bare LF, and complexity of fabrication. For these reasons, this study was designed to use bare LF for assessment of bacterial disinfection via photocatalysis using *E. coli* as the indicator microorganism. Solar photocatalytic inactivation (SPCI) experiments were performed under simulated irradiation and aqueous medium conditions. Besides kinetics of inactivation, a mechanistic approach was also considered in elucidation of the matrix properties formed via cell lysis.

2. Materials and Methods

2.1. Materials

2.1.1. Indicator Microorganism

Stock solution of *E. coli* K12 (ATCC 23716) was prepared in Luria Bertani medium, displaying an initial count of colony forming units as 10^5–10^6 CFU/mL [35].

2.1.2. Aqueous Matrices

SPCI profiles were followed by considering various aqueous matrices to understand behavior and/or response of *E. coli* under specified reaction conditions. Saline solution (SS) consisting of 0.85% NaCl was used to maintain a survival medium to understand *E. coli* inactivation in the absence of any organic and other inorganic constituents. A synthetic solution matrix comprising major cation (Ca^{2+}, Mg^{2+}, Na^+ and K^+) and anion (e.g., Cl^-, NO_3^-, SO_4^{2-}, $H_2PO_4^-$ and HCO_3^-/CO_3^{2-}) contents of natural waters was prepared and defined as water matrix (WM) condition. Ultrapure water (MQ, resistivity: 18.2 MΩ.cm (at 25 °C) and a TOC < 5 ppb) was selected as the base reaction medium free of any organic and inorganic constituents of natural water conditions, whereas distilled/deionized water (DW, resistivity: 2 MΩ.cm at 25 °C) was used to eliminate the effect of all ionic constituents.

2.1.3. Preparation of the Catalyst

LF nanopowder was prepared by citrate auto-combustion of dry gel obtained from a solution of the corresponding nitrates poured into citric acid solution, as described in our previous work [36]. Briefly, a specific amount of dried La_2O_3 was dissolved in a nitric acid solution (65% m/m) to prepare $La(NO_3)_3 \cdot 6H_2O$. The resulting powder was calcined at 600 °C for 3 h in air. Iron nitrate was dissolved in water (0.1 M) by stirring on a hotplate, and then the solution was poured in citric acid solution, with the molar ratio of iron to citric acid being set at 1:1. Aqueous NH_3 was added slowly until pH 6.8, and the solution turned transparent. The solution was then dehydrated until a brown/orange $LaFeO_3$ gel formed. The dry gel was heated in air to 250 °C to start ignition. The resulting lightweight powder was calcined at 600 °C for 3 h to remove any organic residue and an ochre $LaFeO_3$ powder was obtained after calcination. The XRD pattern of the powder display peaks that are attributed to $LaFeO_3$ orthorhombic perovskite [36], with some degree of broadening resulting from the nanocrystalline nature of the powder, is shown in Supplementary Figure S1. Supplementary Figure S2 also shows a SEM image of LF, where the particles are mainly in the range 30 to 60 nm. Supplementary Figure S3 illustrates the UV-vis diffuse reflectance spectrum of LF powder. The optical band gap energy is determined as 2.5 eV.

2.2. Methodology

2.2.1. Solar Photocatalytic Inactivation of *E. coli*

SPCI experiments were conducted using an Atlas Suntest CPS+ solar simulator (Atlas, IL, USA) equipped with an air-cooled Xenon lamp with emission range of λ = 300–800 nm and I_o = 250 W/m^2. LF dose was kept constant at 0.50 mg/mL for inactivation experiments in the presence of various aqueous medium components. Optimum mixing speed that causes no vortex but ensures homogeneous mixing was properly adjusted. LF dose effect was investigated using 0.25, 0.50, 0.75 and 1.0 mg/mL in SS. All runs were performed individually using 100 mL sample volume. Intra-laboratory calibration experiments revealed an error ≤ 5% in all measurements.

2.2.2. Analytical Methodology

Enumeration of *E. coli*

Enumeration of *E. coli* was assured by the drop plate method [37]. Appropriate serial dilutions were made, and samples were incubated at 44 °C overnight, following which visual counting of the colonies expressed as CFU/mL was performed. Each run was carried out in triplicate. Following bacterial enumeration sampling, total volume of the samples was further filtered through a sequence of 0.45 and 0.20 μm membrane filters prior to analysis.

Spectroscopic Characterization of the Organic Matrix

Organic matter was characterized by a Perkin Elmer Lambda 35 Spectrophotometer for UV-vis spectral features using quartz cells with 1.0 cm path-length. A Perkin Elmer LS 55 Luminescence Spectrometer equipped with a 150 W xenon arc lamp and a red sensitive

photomultiplier tube was used for elucidation of fluorescence features in synchronous scan mode [38]. Synchronous scan mode was performed in an excitation wavelength range of 350–600 nm, with the bandwidth of $\Delta\lambda = 18$ nm between the excitation and emission monochromators. Specified UV-vis parameters were defined as $Color_{436}$, UV_{365}, UV_{280} and UV_{254} considering absorbance values recorded at respective wavelengths as 436, 365, 280 and 254 nm. Specified fluorescence intensity, i.e., FI_{syn}, was the maximum fluorescence intensity measured using synchronous scan mode. Specific UV-vis spectroscopic parameters were defined as the ratio of the specified UV-vis absorbance to DOC contents (m^{-1} L/mg), i.e., $SCoA_{436}$, $SUVA_{365}$, $SUVA_{280}$ and $SUVA_{254}$. Accordingly, specific fluorescence intensity was SFI_{syn}, calculated as FI_{syn} normalized to DOC contents.

Detection of Cellular Contents upon Cell Lysis

A Shimadzu Vwp TOC analyzer was used for the determination of organic carbon contents (DOC, mg/L) in non-purgeable organic carbon mode. Protein contents were elucidated by the Lowry method [39]. The method is based on the reaction of Cu^{2+} with the peptide nitrogen(s) under alkaline conditions, and subsequently with Folin–Ciocalteu reagent, by which phosphomolybdotungstate is reduced to heteropolymolybdenum blue by the copper-catalyzed oxidation of aromatic amino acids. The reactions result in a strong blue color, which depends partly on the tyrosine and tryptophan contents. The concentration of the reduced Folin–Ciocalteu reagent is measured by recording absorbance at a wavelength of 750 nm. K^+ contents were determined according to methodology given in Standard Methods as the 3500-K B Flame Photometric Method. The method is based on the determination of potassium at a wavelength of 766.5 nm.

Additional Techniques

Zeta potential was measured using a Malvern Zetasizer NanoZS instrument. Iron (LOD: 0.05 mg/L) and lanthanum (LOD: 0.1 mg/L) concentrations were determined by using ICP-OES (Perkin Elmer Optima 2100). Anions were determined by ion chromatography (IC) (DIONEX ICX-3000). A Perkin Elmer AAnalyst 300 Atomic Absorption Spectroscopy was also used for Na^+, Ca^{2+} and Mg^{2+} determination [35].

3. Results

3.1. Solar Photocatalytic Inactivation of E. coli Using LaFeO$_3$

3.1.1. Solar Photocatalytic Inactivation of *E. coli* in Saline Solution

SPCI of *E. coli* in SS was performed as a baseline experiment to exclude the presence of all interfering species in reaction medium. Various LF doses (0.25, 0.50, 0.75 and 1.0 mg/mL) in SS were selected to evaluate a working dose for both *E. coli* inactivation as well as elucidation of released organic matrix properties. An LF dose of 0.25 mg/mL expressed considerable enhancement compared to 0.50 and 0.75 mg/mL doses (Figure 1). However, upon increasing the LF dose to 1.0 mg/mL, a "slow down" effect was observed, most possibly due to the diminished light penetration effects in the heterogeneous reaction medium. Efficiency enhancement attained upon the use of a lower dose of LF (0.25 g/mL) could be explained by the "size effect", directing to more pre-adsorption extent, most probably as a single layer of LF particles onto *E. coli* cells, leading to efficient light absorption. On the other hand, a 0.50 mg/mL LF dose was selected to overcome the possible retardation/inhibition effects upon the use of various water matrix conditions.
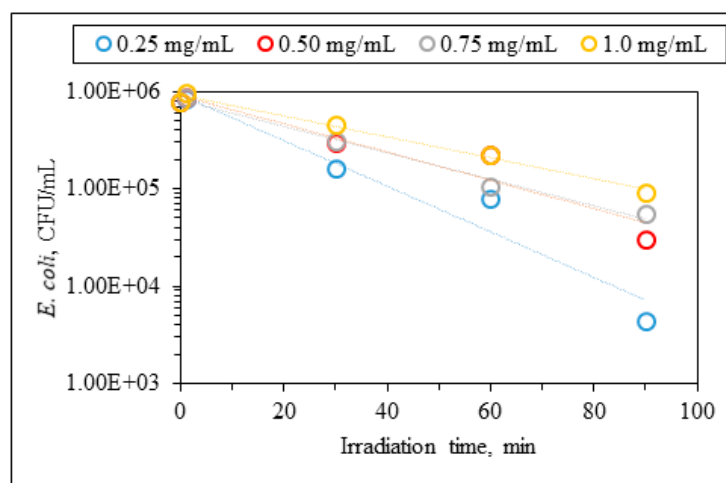
Figure 1. LF dose effect on SPCI of *E. coli* in SS.

Logarithmic decay profiles of *E. coli* cell counts indicated that inactivation kinetics could be well-expressed by the first-order model:

$$\text{Rate (R)} = -dN/dt = kN \tag{1}$$

R: first-order rate (CFU/mL min),
N: *E. coli* count, CFU/mL at time t,
t: irradiation time, min,
k: first-order reaction rate constant, min^{-1}.
Half-life ($t_{1/2}$, min) could easily be calculated by the following equation, $t_{1/2} = 0.692/k$.
SPCI rate constants (k, min^{-1}) were calculated as 5.40E-02, 3.35E-02, 3.13E-02 and 2.46E-02, with respect to increasing LF doses of 0.25, 0.50, 0.75 and 1.0 mg/mL, respectively. Corresponding half-life values ($t_{1/2}$, min) were 12.8, 20.7, 22.1 and 28.2 min.

Due to the lack of any literature findings on the use of bare LF for the inactivation of *E. coli*, no direct comparison was possible. On the other hand, under considerably different operating conditions, a dose of 1.0 mg/mL was employed upon use of $SrTi_{1-x}Fe_x O_{3-\delta}$ and $CoFeO_4$ specimens, revealing 5 and 7 log reductions, respectively [11,15].

3.1.2. Characterization of Released Organic Matrix

Organic matter produced upon photocatalytic treatment of *E. coli* in SS using 0.50 mg/mL LF was followed by the UV-vis and fluorescence spectroscopic measures as well as DOC. It should be mentioned that the determined DOC content was composed of the "formed and simultaneously degraded organic matter" via SPCI treatment of *E. coli*. UV-vis absorbance spectra of the organic matter displayed a continuous declining absorbance with respect to increasing wavelength, resembling almost humic nature [38]. Therefore, humic descriptive parameters were evaluated and presented (Figures 2 and 3).

UV-vis spectroscopic features displayed virtually non-existence of any color-forming chromophoric moieties ($Color_{436}$), but considerable absorption in the UV-region, as expressed by UV parameters. Upon introduction of LF into *E. coli* suspension (t = 0) in the absence of irradiation, dose-dependent variations in release of organic matrix were observed primarily due to the presence of extracellular polymeric substances (EPS) and direct distortion action of LF onto cells.
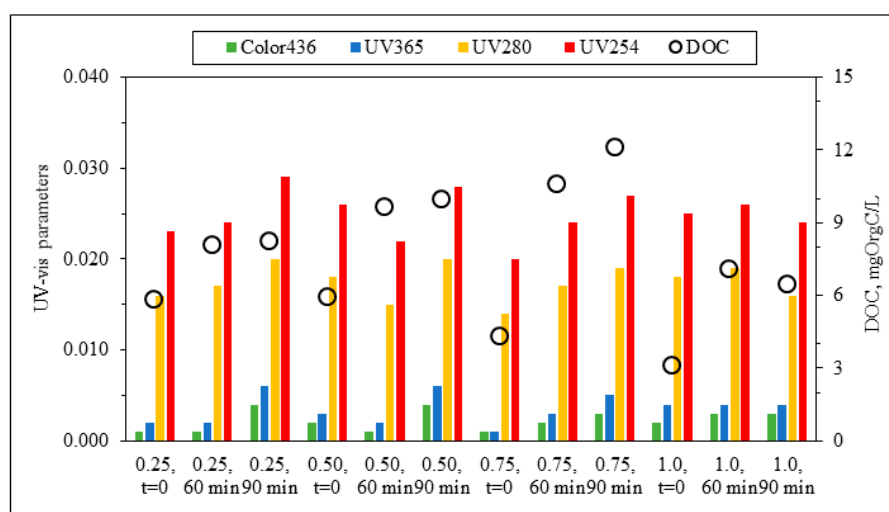
Figure 2. Effect of LF dose on the organic matter formation during *E. coli* inactivation in SS using LF.
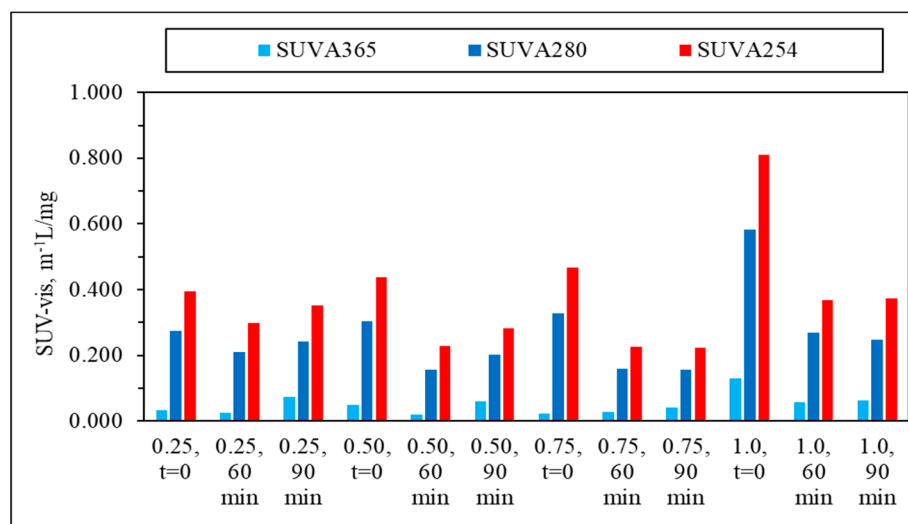

Figure 3. Specific descriptive parameters of the organic matrix derived from *E. coli* inactivation in SS using LF.

Differences in DOC contents could be expressed by instantaneous accumulation of debris under certain time periods (e.g., irradiation time: 45 min) and respective *E. coli* counts. DOC contents increased significantly with respect to irradiation time upon the use of 0.75 mg/mL LF, in comparison to other doses. Irradiation time-dependent release of DOC was not directly correlated with the emergence of UV-absorbing centers, as expressed by UV_{280} and UV_{254} due to the nature of the organics in solution. All of the specific UV parameters were quite low values, indicating the presence of organics expressing more aliphatic nature [40].

3.2. Solar Photocatalytic Inactivation in Various Water Matrices Using $LaFeO_3$
3.2.1. Bacterial Inactivation Profiles

SPCI of *E. coli* was investigated under various solution matrix conditions, such as DW, WM and MQ, in comparison to SS using 0.50 mg/mL LF (Figure 4). Specific interest was devoted to the inactivation profile in SS, excluding the possibility of consecutively operating interfering effects, such as radical scavenging (DW and WM), osmotic pressure (MQ) and competing surface interactions. SCPI profile of *E. coli* in SS could be regarded as

revealing relevant information on the sole role of LF, therefore expressing initial surface interactions, and trends under dark conditions (N_{ss}) were also evaluated.
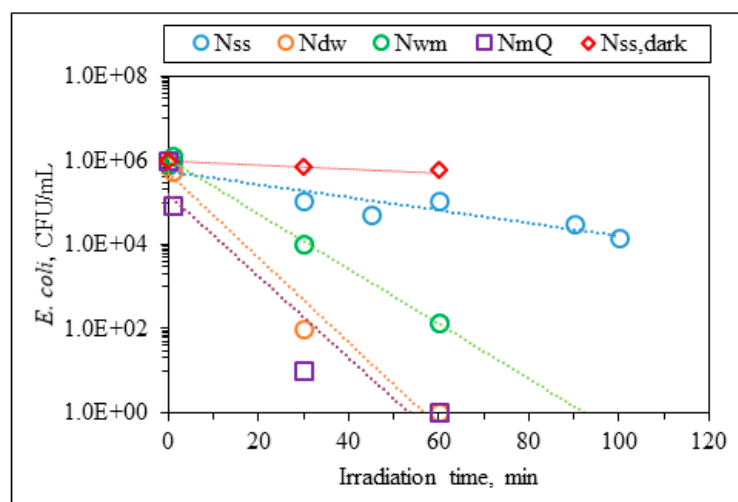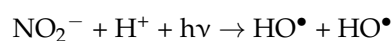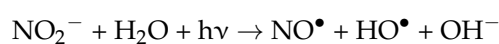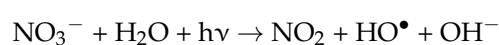

Figure 4. SPCI profiles of *E. coli* (CFU/mL) using LF (0.50 mg/mL) in various aqueous medium conditions (N_{ss}: *E. coli* in saline solution, N_{dw}: *E. coli* in distilled water, N_{wm}: *E. coli* in aqueous solution containing anions and cations, N_{mQ}: *E. coli* in Milli Q water, $N_{ss,dark}$: *E. coli* in saline solution under dark conditions).

The degradation profiles were followed for selected time intervals (0, 30 and 60 min) to investigate the effect of solution matrix conditions. SPCI profiles of *E. coli* (CFU/mL) obeyed first-order kinetic model parameters, which are presented in Table 1 ($R^2 > 0.88$). The highest inactivation rate was achieved in MQ water, followed by DW, WM and SS. MQ water exerted an osmotic pressure effect on the *E. coli* cells along with the destructive action of photocatalysis. *E. coli* inactivation in DW resembled MQ condition as being slightly less pure. Inactivation in WM could be visualized proceeding through various pathways due to the response of the aqueous phase components' irradiation.
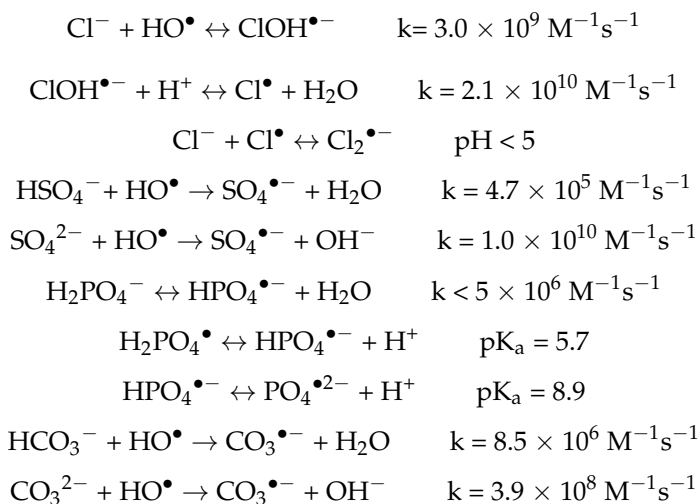
Table 1. First-order kinetic parameters of SPCI of *E. coli*.

E. coli/Aqueous Medium Type	First-Order Kinetic Model Parameters		
	k, min^{-1}	$t_{1/2}$, min	R, CFU/mL min
SS	3.35 E-02	20.7	3.49 E + 04
DW	2.31 E-01	3.0	1.73 E + 05
WM	1.50 E-01	4.6	1.29 E + 05
MQ	3.49 E-01	2.0	3.37 E + 05

In natural waters, common anions, mainly Cl^-, Br^-, CO_3^{2-}, SO_4^{2-} and PO_4^{3-} species, excluding nitrate ($\lambda_{max} = 303$ nm) and nitrite ($\lambda_{max} = 355$ nm), are all known to be transparent to solar radiation. Although common cations, i.e., K^+, Na^+, Ca^{2+} and Mg^{2+}, are also transparent, divalent cations such as Ca^{2+} and Mg^{2+} may take part in complexations reactions, leading to further photochemical reactions:

$$NO_3^- + H_2O + h\nu \rightarrow NO_2 + HO^\bullet + OH^-$$

$$NO_3^- + H^+ + h\nu \rightarrow NO_2^\bullet + HO^\bullet \qquad \Phi = 0.01 \; \lambda = 305 \text{ nm}$$

$$NO_2^- + H_2O + h\nu \rightarrow NO^\bullet + HO^\bullet + OH^-$$

$$NO_2^- + H^+ + h\nu \rightarrow HO^\bullet + HO^\bullet$$

Besides the formation of reactive oxygen species (ROS) during primary steps of photocatalysis, additional formation of $HO^\bullet$ through NO_3^- reactions could facilitate the inactivation rate. A short look at ROS reactions with inorganic species in water would be as follows [41–44]:

$$Cl^- + HO^\bullet \leftrightarrow ClOH^{\bullet-} \qquad k = 3.0 \times 10^9 \text{ M}^{-1}\text{s}^{-1}$$

$$ClOH^{\bullet-} + H^+ \leftrightarrow Cl^\bullet + H_2O \qquad k = 2.1 \times 10^{10} \text{ M}^{-1}\text{s}^{-1}$$

$$Cl^- + Cl^\bullet \leftrightarrow Cl_2^{\bullet-} \qquad pH < 5$$

$$HSO_4^- + HO^\bullet \rightarrow SO_4^{\bullet-} + H_2O \qquad k = 4.7 \times 10^5 \text{ M}^{-1}\text{s}^{-1}$$

$$SO_4^{2-} + HO^\bullet \rightarrow SO_4^{\bullet-} + OH^- \qquad k = 1.0 \times 10^{10} \text{ M}^{-1}\text{s}^{-1}$$

$$H_2PO_4^- \leftrightarrow HPO_4^{\bullet-} + H_2O \qquad k < 5 \times 10^6 \text{ M}^{-1}\text{s}^{-1}$$

$$H_2PO_4^\bullet \leftrightarrow HPO_4^{\bullet-} + H^+ \qquad pK_a = 5.7$$

$$HPO_4^{\bullet-} \leftrightarrow PO_4^{\bullet 2-} + H^+ \qquad pK_a = 8.9$$

$$HCO_3^- + HO^\bullet \rightarrow CO_3^{\bullet-} + H_2O \qquad k = 8.5 \times 10^6 \text{ M}^{-1}\text{s}^{-1}$$

$$CO_3^{2-} + HO^\bullet \rightarrow CO_3^{\bullet-} + OH^- \qquad k = 3.9 \times 10^8 \text{ M}^{-1}\text{s}^{-1}$$

Since all of these reactions would also be simultaneously occurring and light harvesting efficiency of LF could be altered, the overall effect of these $HO^\bullet$-consuming reactions could possibly retard the SPCI rate of *E. coli*.

Common anions such as HCO_3^-, SO_4^{2-} and $H_2PO_4^{2-}$ do not exhibit any direct bactericidal activity, indicating that these common anions do not play any eminent role in inactivation of *E. coli*. Bacteria and photocatalyst surface interactions mainly operate with respect to pH of the reaction medium (pH_{zpc} conditions) and presence of inorganic species. All of the negatively charged constituents of the water matrix would be attracted to the most positively charged LF surface ($pH_{zpc} = 8.9$) through electrostatic interactions, leading to the blockage of the surface for further interactions. These anions could favorably be adsorbed onto the surface of LF through electrostatic interactions and react with photo-generated redox pair (h^+ and $HO^\bullet$), producing $HCO_3^\bullet$, $SO_4^{\bullet-}$ and $H_2PO_4^{\bullet 2-}$ radicals, which are less reactive than h^+ and $HO^\bullet$. $HCO_3^\bullet$ and $SO_4^{\bullet-}$ radicals could enhance inactivation rate, however the formation of $H_2PO_4^{\bullet 2-}$ could exert a retardation effect.

E. coli surface charge is always negative due to the presence of lipopolysaccharides, below which a lipoprotein layer exists on the outer membrane along with adhesive fimbriae. Bacterial cell walls expose numerous carboxyl, phosphate and phenolic types of functional groups to the aqueous phase and are negatively charged at pH values above approximately 2–3 due to deprotonation of these functional groups. The isoelectric point of *E. coli* was reported as pH 5.5 [45].

LF surface charge is dominated by $pH_{zpc} = 8.9$, expressing that LF surface is mostly positively charged at solution pH conditions of pH 6–7, that is being less than pH_{zpc}. Therefore, electrostatic attractions could be expected between the components of the ternary system composed of *E. coli*, organic sub-fractions and LF surface. Since *E. coli* is considerably larger in size (*E. coli* length = 1–2 μm and diameter = 0.5–1 μm), both organic sub-fractions and LF would be directed to the *E. coli* cell surface. During the dynamic experimental conditions, the active driving force would be the electrostatic attraction supported by the continuous stirring of the reaction medium. The working pH conditions of all experiments were almost neutral, therefore electrostatic interaction prevailing between *E. coli* and LF would result in attachment of LF onto *E. coli*. Cell-appendages (i.e., pili (or fimbriae), flagella) could readily overcome initial bacterial-surface repulsions occurring between charged sites [46]. *E. coli* cells could display cell-surface attachment through weak long-range electrostatic and van der Waals forces, and hydrophobic cell-substratum in a reversible manner, however irreversible attachment phase could also be achieved through

stronger forces, such as hydrogen and covalent bonding, and hydrophobic interactions, combined with contributions from cellular surface structures (fimbriae, flagella, polysaccharides, etc.). *E. coli* cell surface coverage by LF particles would enhance the light harvesting capacity of the system, favoring the formation of ROS.

Negative zeta potential values were recorded roughly between –10 and –20 mV. More specifically, the zeta potentials of *E. coli* in SS, DW and WM were –9.91, –14.57 and –12.98 mV, respectively. Therefore, under all experimental conditions, *E. coli* suspension exerted negative charge to further particle interactions. Consequently, these prevailing electrostatic interactions between negatively charged *E. coli* cells with positively charged LF surface and the aqueous medium constituents facilitated the SPCI rate of *E. coli*.

The effect of aqueous medium type in which *E. coli* cells were subjected to irradiation during SPCI using various photocatalyst specimens was highly documented and discussed by Uyguner-Demirel and colleagues [47]. Since phosphate buffer could possibly exert an inhibitory role via various reaction pathways during photocatalysis, use of SS could be accepted as a convenient base medium. LF dose was selected as 0.50 mg/mL to ensure a comparison with the data achieved upon use of LF for successful degradation of humic acids, as reported previously by Turkten and colleagues [8]. Furthermore, SPCI of *E. coli* was investigated in SS to constitute a baseline for further studies using natural organic matter analogue compounds as the major organic consortium of natural waters [48].

In SS solution, first-order kinetic data displayed rate constant as 3.35 E-02 min^{-1}, half-life as 20.7 min and SPCI rate as 3.49 E + 04 CFU/mL min (Table 1). The expected effect of chloride ions upon irradiation additionally during surface attractions could also be visualized with respect to the previously presented information. Dark interactions of *E. coli* and LF resulted in a very low removal (<1 log) (Figure 4).

3.2.2. Effect of Solar Photocatalytic Inactivation on Cellular Constituents Released: Spectroscopic Detection

The released organic matrix was characterized by UV-vis and fluorescence spectroscopic measures (Figures 5–7). UV-vis spectra attained for organic matter in SS displayed a declining profile lacking any specific absorption peak resembling humic matter (Figure 5). A shoulder region in between 230–280 nm could be visualized under all water matrix conditions, indicating the release of aromatic groups. These groups could be attributed to the presence of amino acids with aromatic moieties either due to the presence of EPS or through cell disruption via lysis. It should be indicated that in the presence of ultra-pure water, cell disruption due to osmotic pressure dominates over SPCI destruction. However, for comparison purposes, the extent of destruction in ultra-pure water should also be addressed. Fingerprint of released carbohydrates could not be assessed directly due to the lack of chromophoric groups that do not exhibit any significant absorption in the 210–400 nm region [49].

The similarities in UV absorption spectral features observed under all conditions irrespective of the irradiation periods hold prime importance with respect to the consistency in the presence of recalcitrant organics that could mostly be aliphatic in nature. It should also be emphasized that even upon prolonged irradiation periods, the regularity of the absorbance should be related to the "quasi-equilibrium" between the formation of these organic fractions and removal via SCPI. Nonappearance of color-forming moieties could be explained by the system dynamics devoid of further intra- and/or inter-molecular interactions occurring via various pathways, such as re-arrangements, condensation and even in situ polymerization through radical reactions.
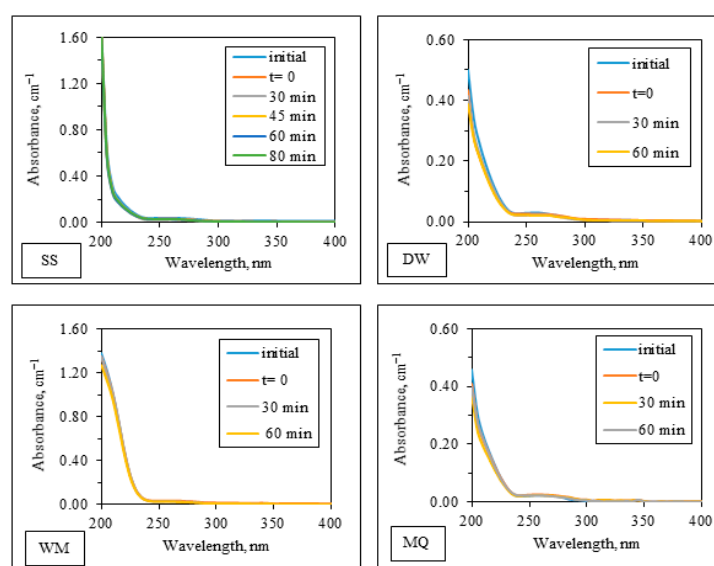
Figure 5. UV-vis absorption spectral features of organic matrix released upon SPCI of *E. coli* in SS, DW, WM and MQ.
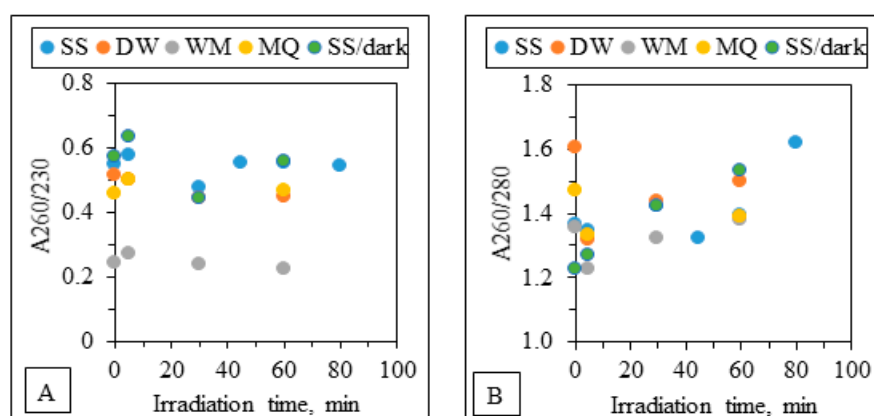

Figure 6. A260/230 (**A**) and A260/280 (**B**) ratios of organic matrix released by SPCI of *E. coli* in the presence of various medium.

The presence of EPS in initial and t = 0 conditions could be assessed by UV-absorbance measurements. EPS were mainly composed of polysaccharides (13%) and protein moieties (55%), and UV-absorption spectra expressed an increasing trend in the wavelength region of 190–230 nm and a shoulder at 260–280 nm [50]. For many organic compounds, peptide bonds in proteins could also absorb in the wavelength range of 200–230 nm along with polysaccharides absorbing at λ = 230 nm. Based on the UV-vis absorption spectra of the samples expressing the presence of all of these compounds, absorbance ratios, e.g., A260/230 and A260/280, could express the significance of the contributing EPS species to the overall absorption trends.
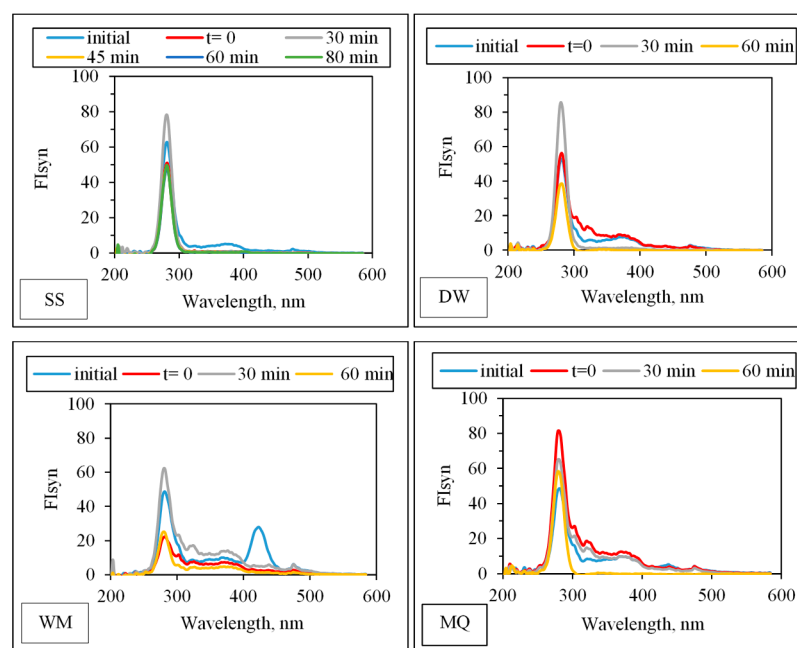
Figure 7. Synchronous scan fluorescence spectral features of organic matrix released upon SPCI of *E. coli* in SS, DW, WM and MQ.

A260/230 ratio < 1.6 indicated poor presence of polysaccharides, whereas >1.9 emphasized the presence of polysaccharides. In a similar manner, A260/280 < 1.6 indicated poor presence of proteins, whereas >1.9 emphasized the presence of proteins. Under initial and t = 0 conditions, all samples expressed A260/230 ratio < 1.6 and A260/280 < 1.6, representing poor presence of carbohydrates and proteins. Furthermore, upon SPCI conditions, the absorbance ratios that reflected almost no change were assessed, and could be considered as insignificant (Figure 6A, B). A260/230 decreasing trend: initial: SS > DW = MQ > WM; t = 0: SS > DW = MQ > WM, A260/280 decreasing trend: initial: DW> MQ > SS = WM; t = 0: SS = DW = MQ > WM.
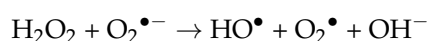
Synchronous scan fluorescence spectra attained for organic matter upon SPCI displayed variations with respect to the solution composition (Figure 7).

Following the major peak with a tailing trend, fluorescence intensities were also detected in the λ_{emis} region between 300 and 500 nm. The well-defined sharp peak recorded at λ_{emis} = 280 ± 1 nm could be related to the release of fluorophores mostly related to the EPS-based proteins with aromatic groups [51]. In WM conditions, under initial conditions, another peak was also recorded at λ_{emis} = 425 nm that could be attributed to the presence of fluorophores originated from organic matrix. In the presence of MQ, the highest peak intensity recorded at t = 0 condition expressed the "burst out" of fluorophores due to osmotic pressure. SFI_{syn} followed an inconsistent trend with respect to the attained variations in both FI_{syn} and respective DOC contents due to the aqueous medium conditions upon an irradiation period of 60 min.

3.2.3. Effect of Solar Photocatalytic Inactivation on Cellular Constituents Released: Analytical Detection

The *E. coli* SPCI process could be visualized as proceeding in two-way processes:

(i)   Outside to inside through cell wall destruction, in which membrane permeability increases and ROS intrusion to the cell interior leads to destruction reactions. Primary ROS active on *E. coli* inactivation was reported as $HO^\bullet$ [3]. H_2O_2 and $O_2^{-\cdot}$ could enter the inner cell via diffusion and could generate OH radical by the Haber-Weiss process, which proceeds very slowly (k < $1M^{-1}s^{-1}$):

$$H_2O_2 + O_2^{\bullet -} \rightarrow HO^\bullet + O_2^\bullet + OH^-$$

(ii) Inside to outside as a consequence of ROS intrusion through cell openings, in which inactivation of protective enzymes (catalase, super oxide dismutase, etc.) leads to various oxidation reactions. Direct action of nanoparticles could be visualized by adsorption onto cells, and through alterations of the cell membrane by lipopolysaccharide degradation, photocatalyst nanoparticles could pass through the pits and be translocated inside the bacterial machinery to carry out antibacterial action through multiple mechanisms such as ROS generation, blockage of cell respiration and inhibition of DNA replication.

It is very well-documented that after the outer membrane distortion and partial decomposition, the reactive species would penetrate to the cytoplasmic membrane, causing the leakage of intracellular content and eventually resulting in cell death. SEM and/or TEM images of bacteria cell destruction using various photocatalysts were very well-documented [2]. Under all conditions due to cell death, release of K^+ as well as biomolecules result in reduced viable and culturable cell counts. Released monosaccharides and amino acids could also serve as nutrients to *E. coli,* however under the high oxidizing conditions, oxidative degradation predominates over post-bacteria growth. Therefore, removal of proteins via uptake mechanism could be omitted. With respect to the literature findings summarized above, release of cellular constituents via SPCI of *E. coli* using LF was assessed by the detection of cell constituents in terms of DOC, protein content and K^+ leakage, and presented in Figures 8–10 prior to and following SPCI.
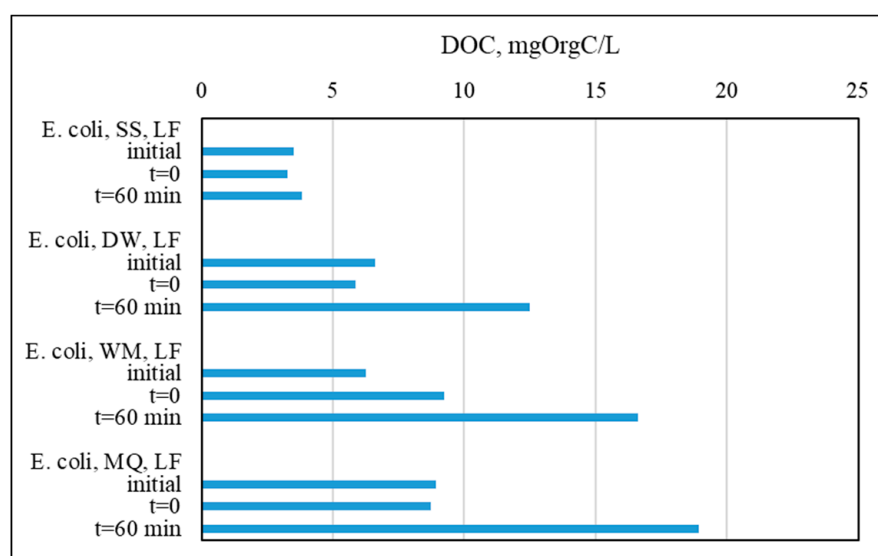

Figure 8. DOC contents of the organic matrix released by SPCI of *E. coli,* in the presence of various medium using LF.

Regarding organic macromolecules, proteins, polysaccharides, lipopolysaccharides and nucleic acids comprise 96% of dry weight, indicating the majority of these components in *E. coli* cells [52]. Therefore, the increase in specified UV-vis parameters as well as DOC content could be attributed to the release of carbohydrates and proteins with aromatic amino acids, such as tryptophan, tyrosine and phenylalanine via cell lysis [53].
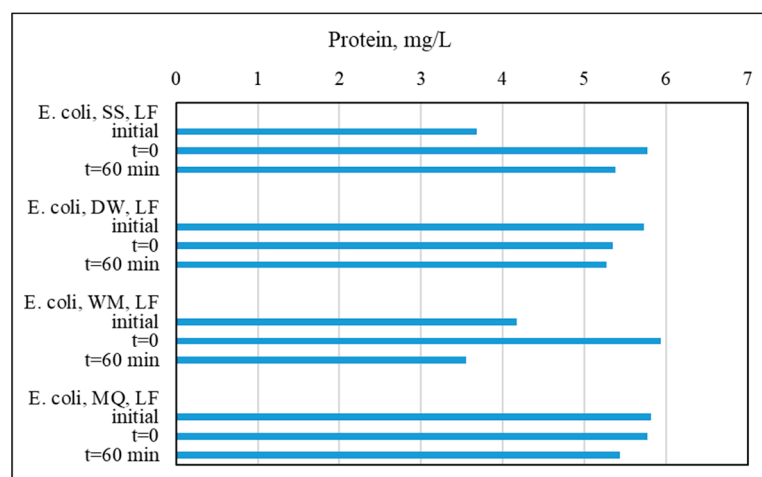
Figure 9. Protein contents of the organic matrix released by SPCI of *E. coli*, in the presence of various medium using LF.
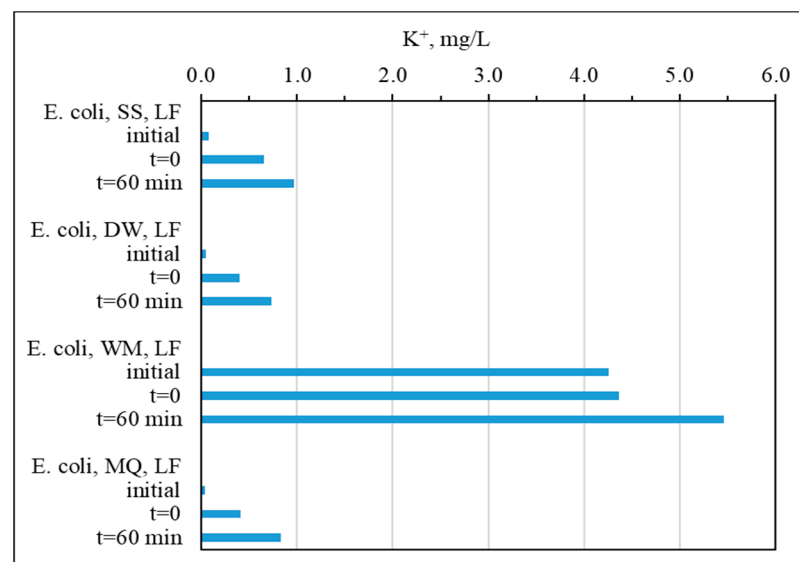

Figure 10. Change in K^+ content under specified experimental conditions prior to and following SPCI of *E. coli* using LF.

Surface coverage of LF revealed initial adsorption percentages of DOC content onto LF as 6% for SS, 11% for DW and 2% for MQ, however WM revealed a distinct profile due to the presence of common anions and cations in WM composition that significantly alters surface interactions between bacteria, LF, as well as bacteria-derived organic constituents. Upon SPCI of *E. coli* for an irradiation period of 60 min, drastic increases in DOC contents were observed in the presence of DW, WM and MQ, whereas a minor change was attained for SS condition (<10% increase in DOC content). The results could be associated with the final bacterial count of each condition upon an irradiation period of 60 min that was found to be 1.15E + 05 CFU/mL for SS, for 1.37E + 02 CFU/mL for WM and <10 CFU/mL for DW and MQ. Removal of *E. coli* cells ended up with the release of all intracellular organic compounds to the reaction medium with contribution to overall DOC content. Under the same conditions, a significant quantity of bacteria was still alive and existent in the presence of SS, whereas almost all bacteria were removed for DW, WM and MQ conditions.

In the presence of SS and WM, an increase was attained at t = 0 condition followed by a decrease upon SPCI of *E. coli* cells under 60 min of irradiation, whereas for DW and MQ water conditions, reduction was attained at t = 0 condition as well as upon SPCI

for t_{irr}: 60 min. Following the SPCI period of 60 min, the reduction in protein content under DW, WM and MQ conditions could be attributed to susceptibility of tryptophan to ROS attack along with tyrosine, histidine, methionine and cysteine [54]. In the presence of SS, protein concentration for t_{irr}: 60 min expressed a higher value compared to initial conditions, which could be related to the presence of a significant amount of bacteria even after 60 min of irradiation, indicating competition between live *E. coli* cells and organics released via lysis of inactivated *E. coli* cells. Significant variations were obtained in WM medium between initial, t = 0 and irradiation period of 60 min conditions as a result of diverse reaction pathways that would possibly withhold and release K^+ ions due to a single positive charge and size effects that influenced surface interactions between LF and protein content. Moreover, $SO_4^{\bullet-}$ radical, which is expected to be formed in WM condition, could react with tyrosine and tryptophan with similar rates (3×10^9 and 2.3×10^9 $M^{-1}s^{-1}$, respectively), therefore leading to the removal of these constituents [42].

Upon SPCI for an irradiation period of 60 min, a significant amount of K^+ content was detected in reaction mediums as a result of the release of cellular K^+ content via cell lysis (Figure 10). Although initial adsorption onto LF surface also ended up with an increase in K^+ content, 60 min of reaction period almost doubled the amount of K^+ content in the presence of all matrices, except for the WM condition, which contains a significant amount of K^+ (3.84 mg/L) as one of the common cation contents of natural water samples. Although the initial K^+ content of WM condition indicated the presence of bacteria-derived K^+ in the reaction medium, interpretation of K^+ content that was either originating from bacteria destruction or present as the constituent of WM composition, and could not be discriminated well. Since K^+ has the tendency to adsorb on the surface of the photocatalyst specimen, adsorptive interactions between matrix-related K^+ and LF brought up the difficulty to follow changes in K^+ content. Further assessment was devoted to the relationship between bacterial inactivation and K^+ release. It could be concluded that a strong correlation ($R^2 > 0.80$) was attained between reduction of bacterial counts and K^+ concentration, excluding data of WM indicating the presence of excess K^+ that could interfere with the overall evaluation of change in K^+ content upon SPCI of *E. coli*.

3.2.4. Photocatalyst Stability, Leaching of Iron and Lanthanum and Ionic Species

Following SPCI of *E. coli* for an irradiation period of 60 min, under all specified conditions, almost no detectable amount of Fe was found in aqueous medium. In a similar manner, leaching of lanthanum was not observed [8]. Furthermore, inorganic anions and cations were also surveyed and verified by IC profiles, as expected.

4. Conclusions

The solar photocatalytic bactericidal performance of a perovskite photocatalyst specimen, such as lanthanum orthoferrites ($LaFeO_3$), to inactivate pathogenic microorganism as *E. coli* in aqueous medium was discussed by addressing the effects of various aqueous medium conditions.

Saline solution was selected as the medium in SPCI of *E. coli* to exclude all interfering species either as ultra-pure water (osmotic pressure) or presence of common water constituents. *E. coli* decay profiles obeyed first-order kinetics of inactivation. First-order rate constant was found to be k = 3.35 E-02 min^{-1}, revealing a half-life of $t_{1/2}$ = 20.7 min and rate of R = 3.49 E + 04 CFU/mL min. Various LF doses (0.25, 0.50, 0.75 and 1.0 mg/mL) in SS were evaluated to select the working dose of 0.50 mg/L.

Characterization of organic matter in the reaction medium consisting of *E. coli* cells, organic sub-fractions formed by cell destruction and $LaFeO_3$ inorganic surface was elucidated by the UV-vis and fluorescence spectroscopic techniques as well as organic carbon content. Further evaluation of photocatalytic cell destruction was followed by monitoring cell components, such as protein and K^+. Upon SPCI for 60 min, a significant amount of K^+ content was detected in reaction medium that proved evidence of cell lysis. Further-

more, release of protein components was also assessed by both UV-vis and fluorescence spectroscopic techniques.

Application of bare LaFeO₃ for solar photocatalytic *E. coli* inactivation in aqueous medium could be a promising treatment alternative. This study demonstrated the role of natural water constituents following a stepwise approach, excluding the role of natural organic matter. Based on the main outcomes of this study, further effort was also devoted to understanding the influence of natural organic matter on solar photocatalytic disinfection of *E. coli* using LaFeO₃, the results of which will be presented in a forthcoming publication.

Supplementary Materials: The following are available online at https://www.mdpi.com/article/10.3390/w13091135/s1, Table S1: Perovskites and perovskite-like materials and their antimicrobial activity properties, Figure S1: Powder XRD pattern of orthorhombic LF, Figure S2: SEM image of LF powder showing the morphology, Figure S3: Diffuse reflectance plot of LF powder.

Author Contributions: Conceptualization, M.B. and I.N.S.; methodology, M.B., I.N.S. and R.P.; validation, M.B., C.S.U.D. and I.N.S.; formal analysis, N.C.B. and E.L.; investigation, N.C.B., R.P., I.N.S. and M.B.; resources, I.N.S. and M.B.; data curation, N.C.B., E.L. and R.P.; writing—original draft preparation, N.C.B., C.S.U.D., R.P., I.N.S. and M.B.; writing—review and editing, N.C.B., C.S.U.D., R.P., I.N.S. and M.B.; supervision, I.N.S. and M.B.; project administration, I.N.S. and M.B. All authors have read and agreed to the published version of the manuscript.

Funding: This research received no external funding.

Institutional Review Board Statement: Not applicable.

Informed Consent Statement: Not applicable.

Data Availability Statement: Not applicable.

Conflicts of Interest: The authors declare no conflict of interest.

References

1. World Health Organization. *Guidelines for Drinking-Water Quality*, 4th ed.; WHO: Geneva, Switzerland, 2017; 631p, ISBN 978-92-4-154995-0.
2. An, T.; Zhao, H.; Wong, P.K. *Advances in Photocatalytic Disinfection*, 1st ed.; Springer: Berlin, Germany, 2017.
3. Cho, M.; Chung, H.; Choi, W.; Yoon, J. Linear correlation between inactivation of E. coli and OH radical concentration in TiO2 photocatalytic disinfection. *Water Res.* **2004**, *38*, 1069–1077. [CrossRef] [PubMed]
4. Li, Q.; Mahendra, S.; Lyon, D.Y.; Brunet, L.; Liga, M.V.; Li, D.; Alvarez, P.J.J. Antimicrobial nanomaterials for water disin-fection and microbial control: Potential applications and implications. *Water Res.* **2008**, *42*, 4591–4602. [CrossRef] [PubMed]
5. Kubacka, A.; Fernández-García, M.; Colón, G. Advanced Nanoarchitectures for Solar Photocatalytic Applications. *Chem. Rev.* **2011**, *112*, 1555–1614. [CrossRef]
6. Rojas-Cervantes, M.L.; Castillejos, E. Perovskites as Catalysts in Advanced Oxidation Processes for Wastewater Treatment. *Catalisys* **2019**, *9*, 230. [CrossRef]
7. Venkatesh, R.; Dhananjay, N.; Sateesh, M.K.; Shabaaz Begum, J.P.; Yashodha, S.R.; Nagabhushana, H.; Shivakumara, C. Effect of Li, Na, K cations on photoluminescence of GdAlO3:Eu3+ nanophosphor and study of Li cation on its antimicrobial ac-tivity. *J. Alloy. Compd.* **2018**, *732*, 725–739. [CrossRef]
8. Turkten, N.; Sora, I.N.; Tomruk, A.; Bekbolet, M. Photocatalytic Degradation of Humic Acids Using Lafeocatal. *Catalisys* **2018**, *8*, 630. [CrossRef]
9. Chu, Y.; Tan, X.; Shen, Z.; Liu, P.; Han, N.; Kang, J.; Duan, X.; Wang, S.; Liu, L.; Liu, S. Efficient removal of organic and bacterial pollutants by Ag-La0.8Ca0.2Fe0.94O3-δ perovskite via catalytic peroxymonosulfate activation. *J. Hazard. Mater.* **2018**, *356*, 53–60. [CrossRef] [PubMed]
10. Ravichandran, A.T.; Srinivas, J.; Karthick, R.; Manikandan, A.; Baykal, A. Facile combustion synthesis, structural, mor-phological, optical and antibacterial studies of Bi1−xAlxFeO3 (0.0 ≤ x ≤ 0.15) nanoparticles. *Ceram. Int.* **2018**, *44*, 13247–13252. [CrossRef]
11. Wang, T.; Jiang, Z.; An, T.; Li, G.; Zhao, H.; Wong, P.K. Enhanced Visible-Light-Driven Photocatalytic Bacterial Inactivation by Ultrathin Carbon-Coated Magnetic Cobalt Ferrite Nanoparticles. *Env. Sci. Technol.* **2018**, *52*, 4774–4784. [CrossRef]
12. Noreen, Z.; Ahmad, I.; Siddiqui, F.; Ziya, A.B.; Abbas, T.; Bokhari, H. Size dependent structural, anti-bacterial and an-ti-biofilm properties of Er doped Li-Ni ferrites synthesized by the sol-gel auto-combustion route. *Ceram. Int.* **2017**, *43*, 10784–10790. [CrossRef]
13. Singh, C.; Wagle, A.; Rakesh, M. Doped LaCoO3 perovskite with Fe: A catalyst with potential antibacterial activity. *Vaccine* **2017**, *146*, 468–473. [CrossRef]

14.　Sobhani-Nasab, A.; Zahraei, Z.; Akbari, M.; Maddahfar, M.; Hosseinpour-Mashkani, S.M. Synthesis, characterization, and antibacterial activities of ZnLaFe 2 O 4 /NiTiO 3 nanocomposite. *J. Mol. Struct.* **2017**, *1139*, 430–435. [CrossRef]

15.　Zhang, L.; Tan, P.Y.; Chow, C.L.; Lim, C.K.; Tan, O.K.; Tse, M.S.; Sze, C.C. Antibacterial activities of mechanochemically synthesized perovskite strontium titanate ferrite metal oxide. *Colloids Surf. A Phys. Eng. Asp.* **2014**, *456*, 169–175. [CrossRef]

16.　Satheeshkumar, M.K.; Ranjith Kumar, E.; Srinivas, C.; Suriyanarayanan, N.; Deepty, M.; Prajapat, C.L.; Chandrasekhar Rao, T.V.; Sastry, D.L. Study of structural, morphological and magnetic properties of Ag substituted cobalt ferrite nanoparticles prepared by honey assisted combustion method and evaluation of their antibacterial activity. *J. Magnet. Aip. Conf. Proc.* **2019**, *469*, 691–697. [CrossRef]

17.　Schwarz-Linek, J.; Arlt, J.; Jepson, A.; Dawson, A.; Vissers, T.; Miroli, D.; Pilizota, T.; Martinez, V.A.; Poon, W.C.K. Esch-erichia coli as a model active colloid: A practical introduction. *Colloid. Surface. B* **2016**, *137*, 2–16. [CrossRef]

18.　Toan, N.; Saukko, S.; Lantto, V. Gas sensing with semiconducting perovskite oxide Lafeophys. *B Condens. Matter* **2003**, *327*, 279–282. [CrossRef]

19.　Di Bartolomeo, E.; Kaabbuathong, N.; D'Epifanio, A.; Grilli, M.L.; Traversa, E.; Aono, H.; Sadaoka, Y. Nano-structured perovskite oxide electrodes for planar electrochemical sensors using tape casted YSZ layers. *J. Eur. Ceram. Soc.* **2004**, *24*, 1187–1190. [CrossRef]

20.　Spinicci, R.; Tofanari, A.; Faticanti, M.; Pettiti, I.; Porta, P. Hexane total oxidation on LaMO3 (M = Mn, Co, Fe) perov-skite-type oxides. *J. Mol. Catal. A Chem.* **2001**, *176*, 247–252. [CrossRef]

21.　Xu, J.-J.; Wang, Z.-L.; Xu, D.; Meng, F.-Z.; Zhang, X.-B. 3D ordered macroporous LaFeO3 as efficient electrocatalyst for Li–O2 batteries with enhanced rate capability and cyclic performance. *Energy Env. Sci.* **2014**, *7*, 2213–2219. [CrossRef]

22.　Pelosato, R.; Carrara, V.; Natali Sora, I. Enhanced photocatalytic degradation of ibuprofen in aqueous solution under visible-light irradiation: Effects of LaFeO3 and Cu-doped LaFeOChem. *Eng. Transact.* **2019**, *73*, 181–186.

23.　Natali Sora, I; Fontana, F.; Passalacqua, R.; Ampelli, C.; Perathoner, S.; Centi, G.; Parrino, F.; Palmisano, L. Photoelec-trochemical properties of doped lanthanum orthoferrites. *Electrochim. Acta* **2013**, *109*, 710–715. [CrossRef]

24.　Li, S.; Jing, L.; Fu, W.; Yang, L.; Xin, B.; Fu, H. Photoinduced charge property of nanosized perovskite-type LaFeO3 and its relationships with photocatalytic activity under visible irradiation. *Mater. Res. Bull.* **2007**, *42*, 203–212. [CrossRef]

25.　Parida, K.; Reddy, K.; Martha, S.K.; Das, D.; Biswal, N. Fabrication of nanocrystalline LaFeO3: An efficient sol–gel auto-combustion assisted visible light responsive photocatalyst for water decomposition. *Int. J. Hydrog. Energy* **2010**, *35*, 12161–12168. [CrossRef]

26.　Iervolino, G.; Vaiano, V.; Sannino, D.; Rizzo, L.; Ciambelli, P. Photocatalytic conversion of glucose to H2 over LaFeO3 perovskite nanoparticles. *Chem. Eng. Transact.* **2016**, *47*, 283–288.

27.　Su, H.; Jing, L.; Shi, K.; Yao, C.; Fu, H. Synthesis of large surface area LaFeO3 nanoparticles by SBA-16 template method as high active visible photocatalysts. *J. Nanoparticle Res.* **2010**, *12*, 967–974. [CrossRef]

28.　Wang, K.; Niu, H.; Chen, J.; Song, J.; Mao, C.; Zhang, S.; Gao, Y. Immobilizing LaFeO 3 nanoparticles on carbon spheres for enhanced heterogeneous photo-Fenton like performance. *Appl. Surf. Sci.* **2017**, *404*, 138–145. [CrossRef]

29.　Sora, I.N.; Fumagalli, D. Fast photocatalytic degradation of pharmaceutical micropollutants and ecotoxicological effects. *Env. Sci. Pollut. Res.* **2017**, *24*, 12556–12561. [CrossRef]

30.　Wheeler, G.P.; Baltazar, V.U.; Smart, T.J.; Radmilovic, A.; Ping, Y.; Choi, K.-S. Combined Theoretical and Experimental Investiga-tions of Atomic Doping To Enhance Photon Absorption and Carrier Transport of LaFeO3 Photocathodes. *Chem. Mater.* **2019**, *31*, 5890–5899. [CrossRef]

31.　Dong, S.; Xu, K.; Tian, G. Photocatalytic activities of LaFe1−xZnxO3 nanocrystals prepared by sol–gel auto-combustion method. *J. Mater. Sci.* **2009**, *44*, 2548–2552. [CrossRef]

32.　Liang, Q.; Jin, J.; Liu, C.; Xu, S.; Li, Z. Constructing a novel p-n heterojunction photocatalyst LaFeO 3 /g-C 3 N 4 with enhanced visible-light-driven photocatalytic activity. *J. Alloy. Compd.* **2017**, *709*, 542–548. [CrossRef]

33.　Peng, Q.; Wang, J.; Feng, Z.; Du, C.; Wen, Y.; Shan, B.; Chen, R. Enhanced photoelectrochemical water oxidation by fab-rication of p-LaFeO3/n-Fe2O3 heterojunction on hematite nanorods. *J. Phys. Chem. C* **2017**, *121*, 12991–12998. [CrossRef]

34.　Ye, Y.; Yang, H.; Li, R.; Wang, X. Enhanced photocatalytic performance and mechanism of Ag-decorated LaFeO3 nano-particles. *J. Sol-Gel Sci. Technol.* **2017**, *82*, 509–518. [CrossRef]

35.　*Standard Methods for the Examination of Water and Wastewater*, 22nd ed.; American Water Works Association: Washington, DC, USA, 2012.

36.　Caronna, T.; Fontana, F.; Sora, I.N.; Pelosato, R. Chemical synthesis and structural characterization of the substitution compound LaFe1−xCuxO3 (x = 0–0.40). *Mater. Chem. Phys.* **2009**, *116*, 645–648. [CrossRef]

37.　Alrousan, D.M.A.; Polo-López, M.I.; Dunlop, P.S.M.; Fernández-Ibáñez, P.; Byrne, J.A. Solar photocatalytic disinfection of water with immobilized titanium dioxide in re-circulating flow CPC reactors. *Appl. Catal. B Environ.* **2012**, *128*, 126–134. [CrossRef]

38.　Uyguner-Demirel, C.; Bekbolet, M. Significance of analytical parameters for the understanding of natural organic matter in relation to photocatalytic oxidation. *Chemosphere* **2011**, *84*, 1009–1031. [CrossRef] [PubMed]

39.　Lowry, O.H.; Rosebrough, N.J.; Farr, A.L.; Randall, R.J. Protein measurement with the Folin phenol reagent. *J. Biol. Chem.* **1951**, *193*, 265–275. [CrossRef]

40.　Bekbolet, M.; Sen-Kavurmaci, S. The effect of photocatalytic oxidation on molecular size distribution profiles of humic acid. *Photochem. Photobiol. Sci.* **2015**, *14*, 576–582. [CrossRef]

41. Black, E.D.; Hayon, E. Pulse radiolysis of phosphate anions H2PO4-, HPO42-, PO43-, and P2O74- in aqueous solutions. *J. Phys. Chem.* **1970**, *74*, 3199–3203. [CrossRef]

42. Neta, P.; Huie, R.E.; Ross, A.B. Rate Constants for Reactions of Inorganic Radicals in Aqueous Solution. *J. Phys. Chem. Ref. Data* **1988**, *17*, 1027–1284. [CrossRef]

43. Uyguner, C.S.; Bekbolet, M. Application of Photocatalysis for the Removal of Natural Organic Matter in Simulated Surface and Ground Waters. *J. Adv. Oxid. Technol.* **2009**, *12*, 87–92. [CrossRef]

44. Vione, D.; Minella, M.; Maurino, V.; Minero, C. Indirect Photochemistry in Sunlit Surface Waters: Photoinduced Production of Reactive Transient Species. *Chem. A Eur. J.* **2014**, *20*, 10590–10606. [CrossRef]

45. Harden, V.P.; Harris, J.O. The isoelectric point of bacterial Cellsj. *Bacteriology* **1953**, *65*, 198–202. [CrossRef]

46. Elbourne, A.; Chapman, J.; Gelmi, A.; Cozzolino, D.; Crawford, R.J.; Truong, V.K. Bacterial-nanostructure interactions: The role of cell elasticity and adhesion forces. *J. Colloid Interface Sci.* **2019**, *546*, 192–210. [CrossRef]

47. Uyguner-Demirel, C.S.; Birben, N.C.; Bekbolet, M. A comprehensive review on the use of second generation TiO2 photo-catalysts: Microorganism inactivation. *Chemosphere* **2018**, *211*, 420–448. [CrossRef]

48. Birben, N.C.; Lale, E.; Pelosato, R.; Cozzarini, L.; Uyguner-Demirel, C.S.; Schmid, C.; Natali Sora, I.; Bekbolet, M. Photo-catalytic bactericidal performance of LaFeO3 under solar light: Role of natural organic matter. **2021**. in preparation.

49. Kaijanen, L.; Paakkunainen, M.; Pietarinen, S.; Jernström, E.; Reinikainen, S.-P. Ultraviolet detection of monosaccharides: Multiple wavelength strategy to evaluate results after capillary zone electrophoretic separation. *Int. J. Electrochem. Sci.* **2015**, *10*, 2950–2961.

50. Trabelski, L.; M'sakni, N.M.; Ouada, H.B.; Bacha, H.; Roudesli, S. Partial characterization of extracellular polysaccharides produced by Cyanobacterium Arthrospira platensis. *Biotechnol. Bioproc. E.* **2009**, *14*, 27–31. [CrossRef]

51. Reynolds, D. Rapid and direct determination of tryptophan in water using synchronous fluorescence spectroscopy. *Water Res.* **2003**, *37*, 3055–3060. [CrossRef]

52. Madigan, M.T.; Martinko, J.M. *Brock Biology of Microorganisms*, 11th ed.; Pearson Education Inc.: Upper Saddle River, NJ, USA, 2006.

53. Nelson, D.L.; Cox, L. *Principles of Biochemistry*, 4th ed.; W.H. Freeman: New York, NY, USA, 2004.

54. Ronsein, G.E.; Oliveira, M.C.B.; Miyamoto, S.; Medeiros, M.H.G.; Di Mascio, P. Tryptophan oxidation by singlet molecular oxygen [O2 (1Δg)]: Mechanistic studies using 18O-labeled hydroperoxides, mass spectrometry, and light emission measurements. *Chem. Res. Toxicol.* **2008**, *21*, 1271–1283. [CrossRef] [PubMed]